ESO Science Archive Facility - Phase 3 Data Release Description

ESO programme MAGIC: MUSE gAlaxy Groups In COSMOS - A survey to probe the impact of environment on galaxy evolution over the last 8 Gyr, Data Release DR...

provided by Benoît Epinat, submitted on 2024-04-18, published on 2024-04-22

The MUSE gAlaxy Groups in COSMOS (MAGIC) survey

Abstract

This document describes the data release of the "MUSE gAlaxy Groups in Cosmos" (MAGIC) survey that was built to study the impact of environment on galaxy evolution down to low stellar masses over the last 8 Gyr.

The MAGIC survey was conducted with the Multi Unit Spectroscopic Explorer (MUSE) instrument at the ESO/VLT between 2014 and 2019 as part of the ESO MUSE-Guaranteed Time Observations program "*HOW DID ENVIRONMENT AFFECT GALAXY EVOLUTION OVER THE PAST 8 GYR?*" (PI: T. Contini).

This data release consists of 18 datacubes, observed from 1 to 10 hours using the wide-field mode (1 square arcminute sky coverage per field), with a spectral sampling of 1.25 Angstroms and a spatial sampling of 0.2 arcsecond. The datacubes cover the wavelength range between 4700 and 9350 Angstroms and have an image quality better than 0.7'' FWHM owing to good observing conditions and/or to the use of adaptive optics. They reach a median point source flux limit of unresolved emission line of 3.6×10^{-19} erg s^{-1} cm^{-2} at 3σ and a median point source magnitude limit of 28.6 at 5σ. The datacubes target 15 known massive structures at intermediate redshift ($0.3 < z < 0.8$), 14 of which being located in the COSMOS (Knobel et al. 2012) field (RA=150 deg, DEC=2.27 deg) and one in the VVDS (Cucciati et al. 2010) field (RA=36.7 deg, DEC=-4.4 deg).

A detailed description of this dataset and of the sample of objects drawn from the 17 datacubes within the COSMOS field is described in detail in the paper *MAGIC: MUSE gAlaxy Groups In COSMOS - A survey to probe the impact of environment on galaxy evolution over the last 8 Gyr, Epinat et al., A&A, 683, A205 (2024)*, where redshifts for 1419 sources have been securely measured, representing an increase of about 5 times of the number of secure redshifts compared to previous spectroscopic campaigns on the COSMOS field over the MAGIC footprint. The results of this paper suggest that galaxies are preprocessed in groups of increasing mass before entering rich groups and clusters.

The catalogs of detected sources and groups are available through CDS https://cdsarc.cds.unis-tra.fr/viz-bin/cat/J/A+A/683/A205.

The only datacube in the VVDS field (VGr189) is not analyzed in Epinat et al. (2024) but is provided in this data release for completeness.

Overview of Observations

The observations were carried out as part of MUSE-Guaranteed Time Observations over 10 observing periods from December 2014 (P94) until May 2019 (P103), corresponding to the programs 094.A-0247, 095.A-0118, 096.A-0596, 097.A-0254, 098.A-0017, 099.A-0246, 0100.A-0607, 0101.A-0282, 0102.A-0327, 0103.A-0563.

Fourteen structures were chosen from the zCOSMOS 20k group catalog (Knobel et al. 2012) and one from the VIMOS Very Deep Survey (VVDS) group catalog (Cucciati et al. 2010), all within the redshift range $0.3 < z < 0.8$. These groups catalogs were first used to select groups containing at least five spectroscopic members within one single MUSE field. Eleven groups were chosen with this strategy, among which, five were observed from P94 to P96, with exposures ranging from about 2 to 10 h. After these periods, the observing strategy was refined to prepare for adaptive optics (AO) assisted observations: in P97 to P99, 1 h snapshots on fields were observed with suitable tip-tilt stars to further select the most promising candidates for subsequent AO observations. With this aim, additional fields were chosen by allowing for mosaicking around large overdensities identified from the zCOSMOS 20k group catalog (Knobel et al. 2012) and COSMOS2015 photometric catalog (Laigle et al. 2016). This added four new fields on two main structures, including a new one (CGr32). After this snapshot campaign, four groups were discarded from further AO assisted observations, starting in P100. Three more groups were finally added from the COSMOS Wall group catalog (Iovino et al. 2016) for the last P102 and P103 periods. We selected the richest groups that could be observed with AO and that had X-ray counterparts (Gozaliasl et al. 2019), since the densest groups we previously observed were fulfilling these criteria. The final

dataset is composed of 18 fields, 17 of which are located in the COSMOS field, as shown in Fig. 1, and one field in the VVDS area shown in Fig. 2.

Table 1: Log of observations for all MAGIC fields. (1) Name of the observed field, the field identifier corresponds to the targeted group ID either from Knobel et al. (2012) for CGr ([CMI2010] in Simbad) groups, or from Cucciati et al. (2010) for the VGr ([CMI2010] in Simbad) group. -Mi suffixes correspond to sub-fields of the mosaic. (2), (3) Equatorial J2000 right ascension and declination of the field center. (4) MUSE field orientation measured from North to East. (5) Total on-source exposure time, the value in parentheses with bold fonts corresponds to the exposure time obtained using the adaptive optics mode, if any. (6) ESO periods of observations, bold fonts correspond to AO observations. (7) Full width at half maximum at 7000 Angstroms inferred from the Moffat point spread function fit in arcseconds.

Field name (1)	R.A. (Deg) (2)	Dec. (Deg) (3)	Orientation (Deg) (4)	Exposure (hours) (5)	Periods (6)	FWHM (arcsec) (7)
CGr23	149:47:34.7	2:10:06.6	0	1	P98	0.615
CGr26	150:29:30.8	2:04:14.5	35	1	P98	0.586
CGr28	150:13:31.6	1:48:43.8	-10	4.33 (**3.33**)	P98, **P102**	0.569
CGr30	150:08:26.1	2:04:05.5	10	9.75	P94, P95	0.588
CGr32-M1	149:55:15.9	2:31:52.4	30	4.33 (**3.33**)	P97, **P100**	0.480
CGr32-M2	149:56:02.4	2:31:22.3	30	4.33 (**3.33**)	P97, **P101**	0.490
CGr32-M3	149:55:08.1	2:30:46.9	30	4.33 (**3.33**)	P97, **P101**	0.546
CGr34	149:51:23.2	2:29:27.0	-4	5.25	P94, P96	0.571
CGr35	150:00:21.6	2:27:23.4	30	4.67 (**4.67**)	**P102**, **P103**	0.555
CGr51	149:58:53.1	1:47:57.0	-30	1	P99	0.577
CGr61	149:43:34.1	1:55:06.9	-40	1	P98	0.596
CGr79	149:49:07.5	1:49:17.9	-20	4.33 (**3.33**)	P98, **P100**	0.501
CGr84-M1	150:03:02.2	2:35:47.1	0	5.25	P94, P96	0.532
CGr84-M2	150:03:32.7	2:36:44.0	0	4.67 (**4.17**)	P97, **P102**	0.608
CGr87	150:01:30.1	2:21:27.8	-20	2.67 (**2.67**)	**P103**	0.540
CGr114	149:59:55.0	2:15:31.6	-15	4.11 (**2.17**)	P94, **P102**	0.588
CGr172	150:10:15.8	2:31:22.7	0	4.67 (**4.67**)	**P103**	0.481
VGr189	36:41:36.0	-4:23:32.4	18	2.25	P96	0.600

Dark nights and good seeing conditions were requested. For each field, observations were split into observing blocks (OBs) of about 1 h execution time. OBs consist in four 900 s (or 600 s) individual exposures with a small spatial dithering pattern (<0.3") and a 90° rotation of the field between each individual exposure in order to reduce the systematics induced by the integral field unit (IFU) image slicer. The central coordinates of the fields, their rotation angle with respect to the North, and their on-source exposure time and corresponding observing periods are summarized in Table 1. The position of the center of MUSE fields have been refined to optimize the number of sources within the field belonging to each targeted groups and, for groups observed with AO, to get a suitable tilt-tilt star. The aimed exposure time is about 4 to 5 hours per field. The various exposure times for the various fields result from the target selection and observing strategy presented above, as well as from observing constraints in program completion for the latest observed field (CGr87). All data were acquired in Wide Field Mode, using either standard seeing-limited or AO assisted observations with the GALACSI AO facility (La Penna et al. 2016; Madec et al. 2018). Note that with the laser-assisted AO mode, MUSE spectra have a gap in the 5800–5980 Angstroms wavelength range due to the AO notch filter.

Standard calibrations, including day-time instrument calibrations as well as standard star observations, were used for this program. All science exposures include single internal flat-field exposures taken as night calibrations. These short exposures, taken after each OB or whenever there is a sudden temperature change in the instrument, are used for an illumination correction. These calibrations are important to correct for time and temperature dependence on the flat-field cali-

bration between each slitlet throughout the night. In addition, twilight exposures are taken every few days and are used to produce an on-sky illumination correction between the 24 MUSE channels.

The total exposure time devoted to the program reached 95 h including overheads and 69 h on-source. Half the observations (35 h on-source) have used the AO. Twelve fields have been exposed more than 4 h and among those, only four did not benefit from AO.
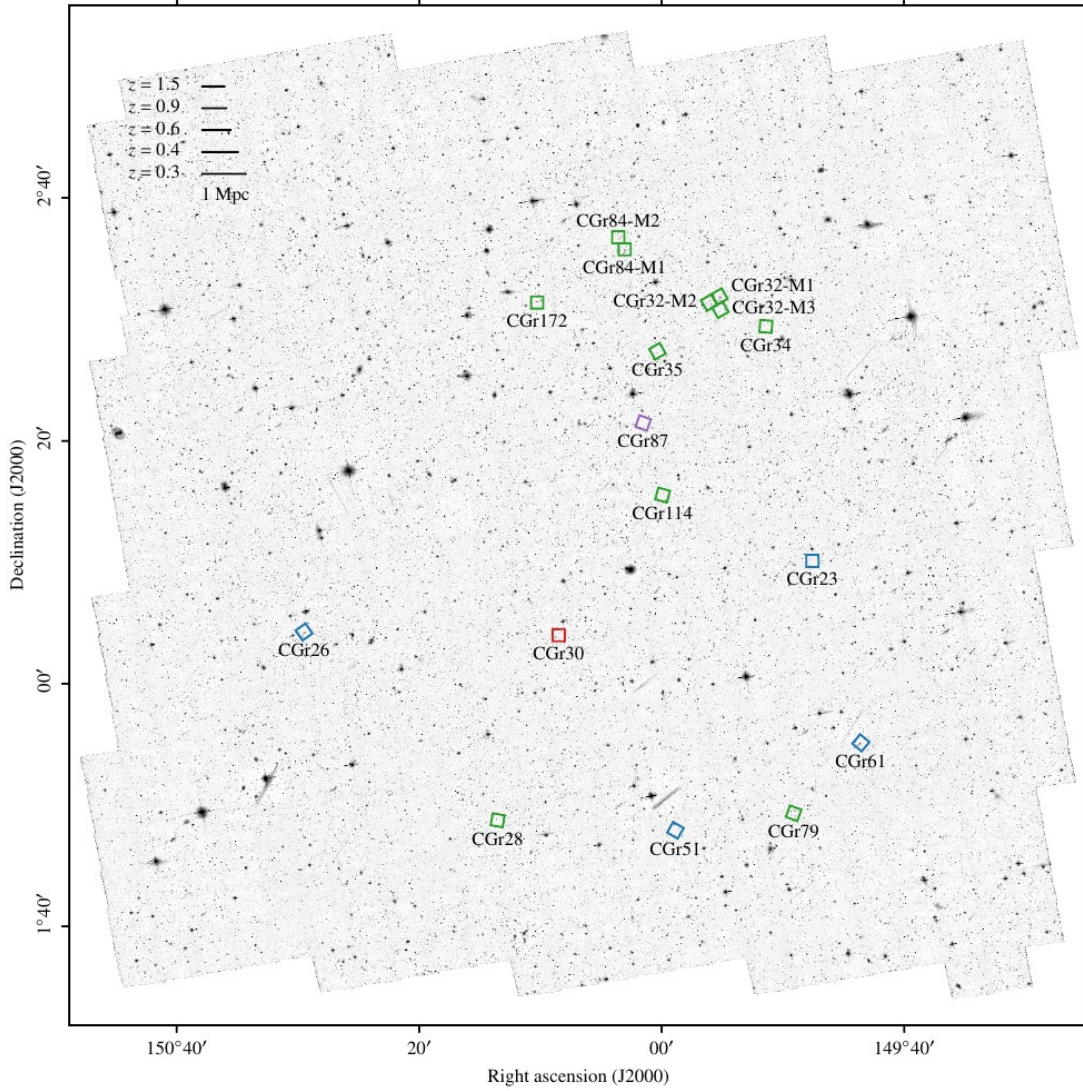

Fig. 1: F814W HST-ACS mosaic over the COSMOS field footprint in logarithmic scale (arbitrary unit), with the 17 MAGIC fields displayed as squares color-coded according to their depth: blue (1 h), purple (2.67 h), green (4.11 h–5.25 h), and red (9.75 h). The scale corresponding to a proper distance of 1 Mpc is indicated for various redshifts in the top-left corner (credits: Epinat et al. 2024).
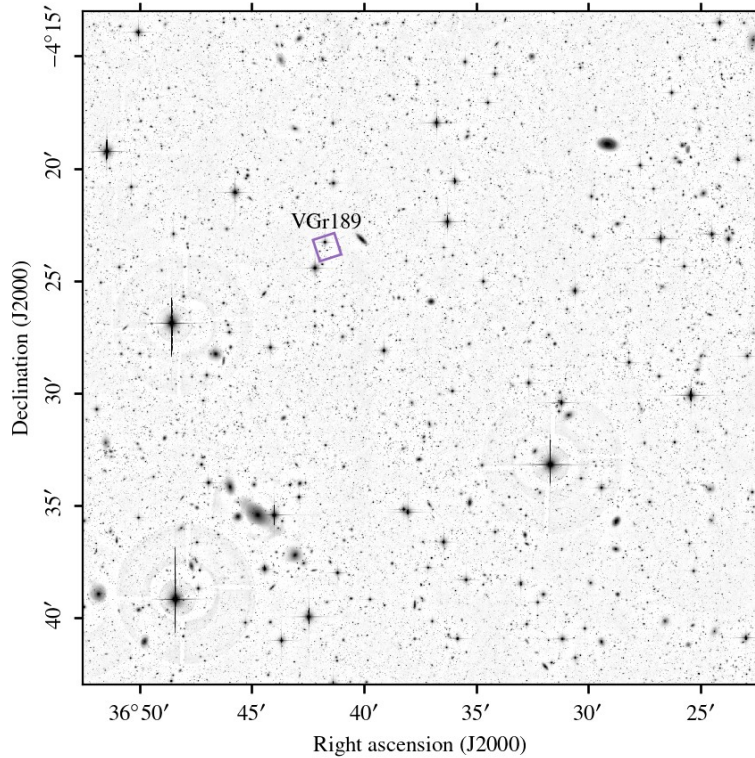
Fig. 2: Fig. 2: CFHTLS image in the i band over a fraction of the VVDS field in logarithmic scale (arbitrary unit), with the VGr189 field displayed.

Release Content

The release is composed of fully reduced MUSE datacubes and corresponding white-light images for each field. Each field covers an area of about 1square arcminute on sky.

Datacubes

For each field, provided datacubes are the combination of datacubes observed over several observing periods. The spectral resolution of the each datacube is R~3000 over the wavelength range 4700-9350 A. The datacubes contain both the data and the associated variance (see Data Format section).

White-light images

For each field, the corresponding white light image is computed as the mean flux over all wavelengths. They are provided in Fig. 12 to Fig. 20.

Release Notes

The data in this release has been introduced and detailed in the MAGIC survey paper (Epinat et al. 2024). Details on target selection, observations and data reduction can be found in Sect. 2.

Data Reduction and Calibration

Each science OB was processed through the MUSE standard pipeline (Weilbacher et al. 2020). Observations with AO were reduced with the v2.4 version of the pipeline, whereas seeing-limited observations used v1.6, except for the CGr30 field which used v1.2. These various versions of the pipeline are the ones that were available at the time the final reduction was performed for each field. Indeed, CGr30 was the first field with completed exposures, and the fields using AO were completed later than those without AO (see Table 1). There are only minor changes between these versions which does not impact the quality of the resulting data cubes.

Data reduction includes all the common steps to process MUSE raw data such as bad pixel tables, bias and dark removals, flat-fielding, wavelength/flux calibration, and sky subtraction. Raw calibration exposures are combined to produce a master bias, master flat and trace table which locates the edges of the slices on the detectors, as well as the wavelength solution for each observing night. These calibrations are then applied on all the raw science exposures to produce a pixel table without any interpolation. A bad pixel map is used to reject known detector defects, and we make use of the geometry table created once for each observing run to precisely locate the slices from the 24 detectors over the MUSE FoV. Twilight exposures and night-time internal flat calibrations are used for additional illumination correction. Pixel tables are then flux-calibrated and telluric-corrected using standard star exposures taken at the beginning/end of the night. In the case of AO-assisted observations laser-induced Raman lines are also subtracted.

Sky subtraction was applied on each individual exposure. The offsets of each single datacube were computed using stars located in the FoV in order to combine the individual pixel tables into the final datacube.

Sky subtraction was further improved by applying the Zurich Atmosphere Purge (ZAP) software (Soto et al. 2016) on the final data cube. ZAP performs a subtraction of remaining sky residuals based on a Principal Component Analysis of the spectra in the background regions of the data cube which has been shown to remove most of the systematics, in particular towards the redder wavelengths. Data reduction produces science-ready data and variance cubes with spatial and spectral sampling of 0.2" and 1.25A, respectively, in the spectral range 4700-9350A.

Data Quality

For each field, the spatial PSF was measured on each final datacube using objects identified as stars in each field. For field CGr87, one bright unresolved object at $z \sim 2.67$ was used in addition to three potential stellar sources having z=0 with a poor redshift confidence due to a very low brightness. We collapse the reduced datacube over 100A to create 6"x6" images around each star every 100A , and model them using a flat background and a 2D circular Moffat function.

A linear fit is then performed through all measurements after excluding the strongest outliers to determine the variation of the PSF FWHM with wavelength, whereas the Moffat index β, that does not vary much with wavelength, is determined as the mean across wavelengths of the measurements that converged, weighted by the inverse of their uncertainty. The parameters of the Moffat functions are stored in the header keywords MOF_FWHM (FWHM at 7000 Angstroms), MOF_DFDL (linear variation with wavelength in arcsecond per micron), and MOF_BETA (β parameter). The PSF FWHM values at 7000 Angstroms are provided in Table 1 for each field and fairly match the values inferred at half the spectral range of the cubes and stored in the SKY_RES header keyword. Spatial resolution (SKY_RES) is quite homogeneous across the MAGIC dataset and vary from 0.48" to 0.61", with a median value of 0.57", thanks to homogeneous observing conditions and AO.

The LSF is relatively stable across different MUSE observations. We used the results from the HUDF fields (Bacon et al. 2017).

The data quality mostly depends on the depth of the data. The typical noise per pixel in each cube in erg s^{-1} cm^{-2} Angstrom^{-1} (PIXNOISE keyword header), inferred from the median of the variance cube, ranges from 3.75×10^{-20} to 1.36×10^{-20} erg s^{-1} cm^{-2} Angstrom^{-1}, with a median value of 1.57×10^{-20} erg s^{-1} cm^{-2} Angstrom^{-1}. Taking seeing into account to perform an optimal extraction for point-like sources, these values correspond to limiting 3σ flux limits of an unresolved emission ranging from 3.2×10^{-19} and 8.4×10^{-19} erg s^{-1} cm^{-2}, with a median of 3.6×10^{-19} erg s^{-1} cm^{-2}, and to limiting AB magnitudes at 5σ (ABMAGLIM header keyword) from 27.6 to 28.8, with a median of 28.6.

The astrometry was matched to the HST-ACS images from the COSMOS2015 catalog (Laigle et al. 2016) for the 17 fields in COSMOS. The accuracy of the astrometry is better than one MUSE pixel (0.2").

Data Format

Files Types

Images and datacubes are in the multi-extension FITS format, with a data in the first extension, and a variance in the second extension. Masked data have NaN values. The primary header of each file contain a WCS extension and a number of keywords, including the spatial PSF model polynomial coefficients (Epinat et al. 2024, Sect. 2.3). The identifiers provided in the primary header (OBJECT keywords) are those of the previously known galaxy groups identified by Knobel et al. (2012) and Cucciati et al. (2010) catalogs, though the MUSE field of view is not always centered on the coordinates provided in these catalogs, therefore RA and DEC keywords in the primary headers do not match these catalog coordinates. For the two groups covered with several fields, a field numbering was added to the identifiers.

These files can be used directly with any FITS reading tool (e.g., fitsio, ds9).

Acknowledgements

White-light images of MAGIC fields

The white-light images obtained from each MUSE datacube corresponding to the various fields are shown hereafter. Both names provided in the OBJECT header keyword and corresponding to those in Fig. 1 and Table. 1 are indicated in the captions.

References

- Bacon et al. 2017, A&A, 608, A1
- Cucciati et al. 2010, A&A, 520, A42
- Epinat et al. 2024, A&A, 683, A205
- Gozaliasl et al. 2019, MNRAS, 483, 3545
- Iovino et al. 2016, A&A, 592, A78
- Knobel et al. 2012, ApJ, 753, 121
- Laigle et al. 2016, ApJS, 224, 24
- La Penna et al. 2016, SPIE Conf. Ser., 9909, 99092Z
- Madec et al. 2018, SPIE Conf. Ser., 10703, 1070302
- Soto et al. 2016, MNRAS, 458, 3210
- Weilbacher et al. 2020, A&A, 641, A28
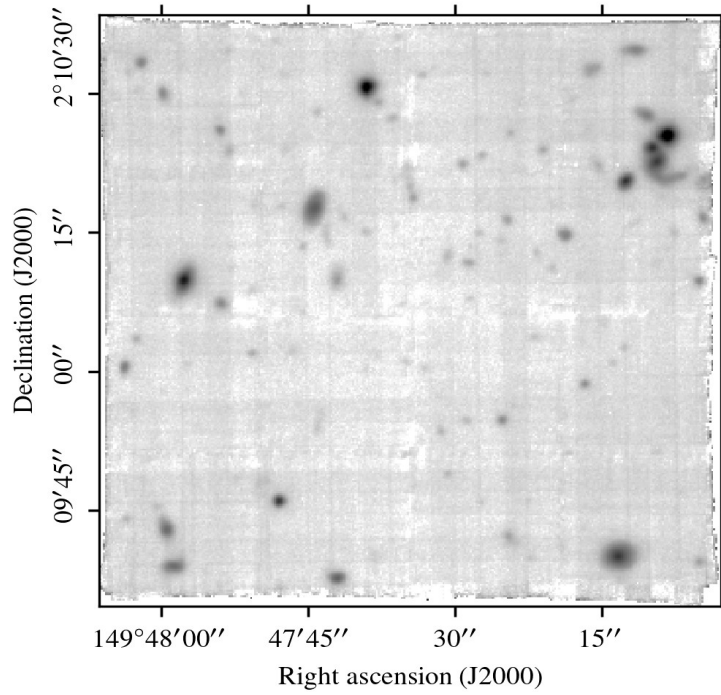
Fig. 3: White-light image in arbitrary logarithmic scale for [KLI2012] 23 (CGr23)
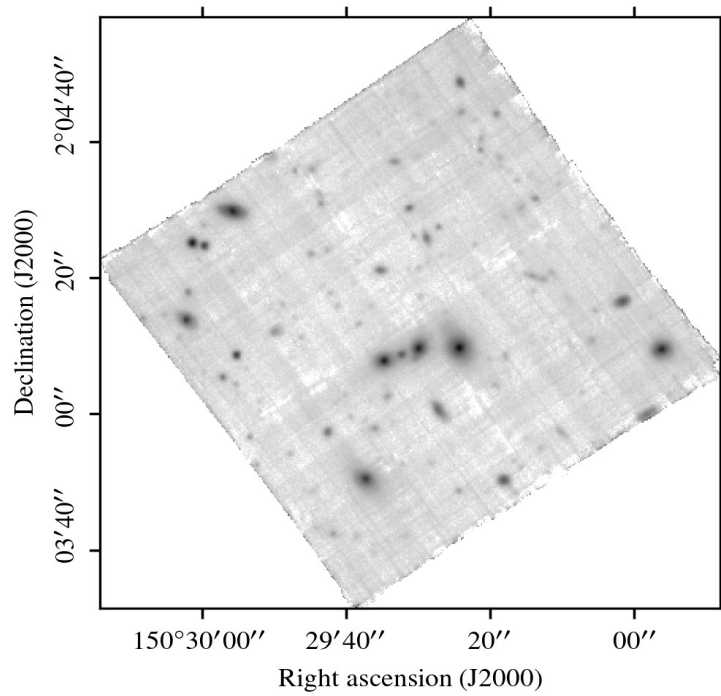
Fig. 4: White-light image in arbitrary logarithmic scale for [KLI2012] 26 (CGr26)
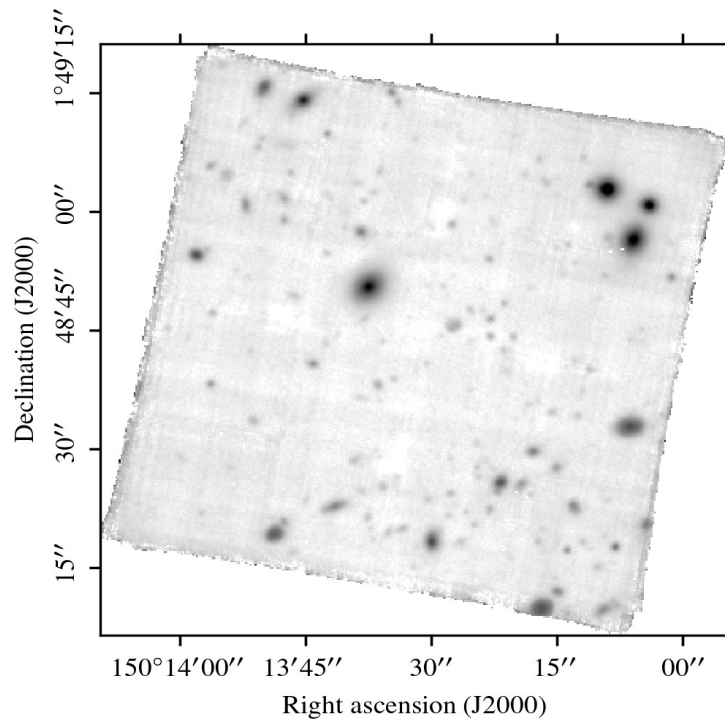
Fig. 5: White-light image in arbitrary logarithmic scale for [KLI2012] 28 (CGr28)
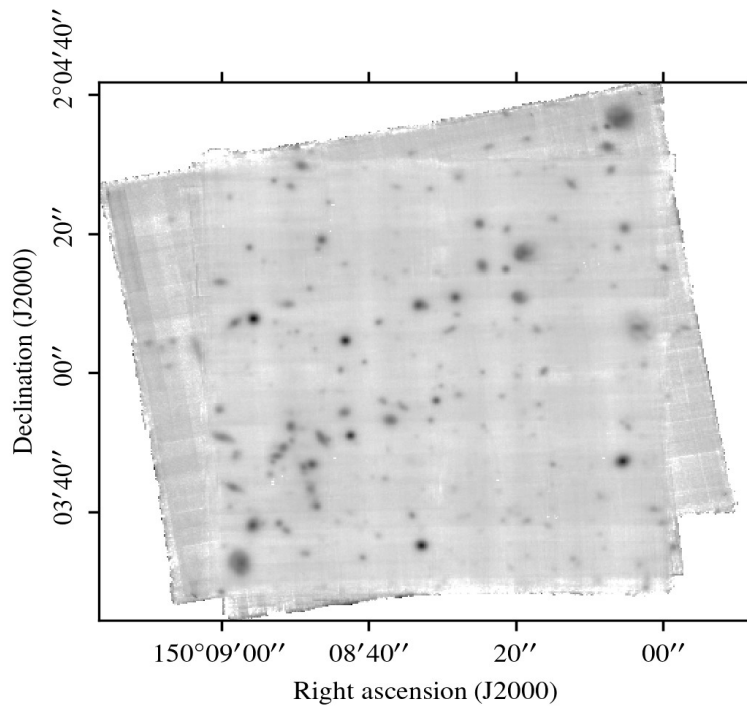

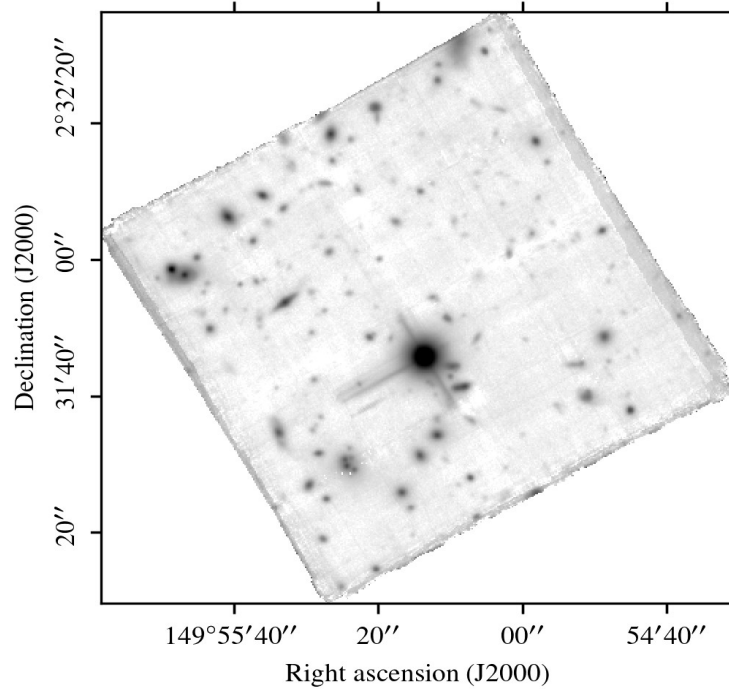*Fig. 6: White-light image in arbitrary logarithmic scale for [KLI2012] 30 (CGr30)*

Fig. 7: White-light image in arbitrary logarithmic scale for [KLI2012] 32 field1 (CGr32-M1)
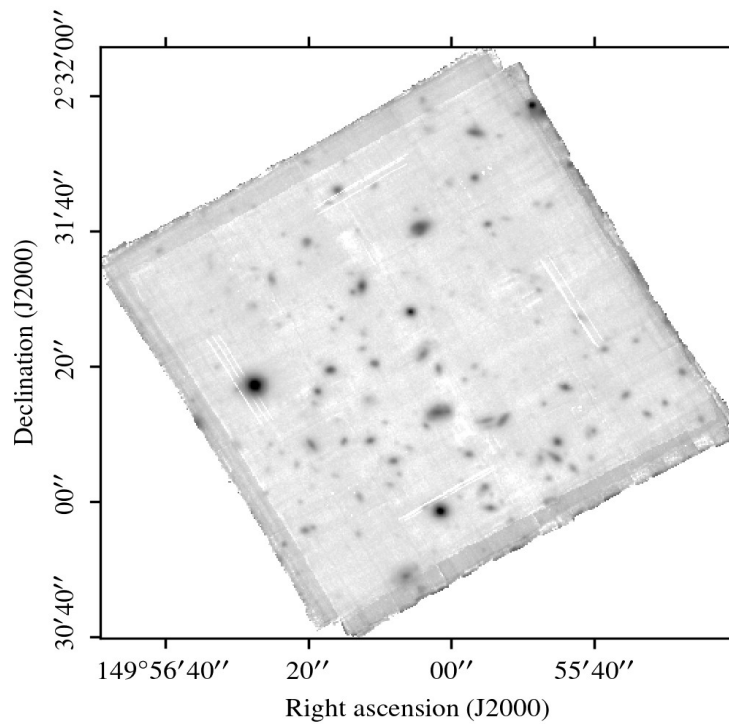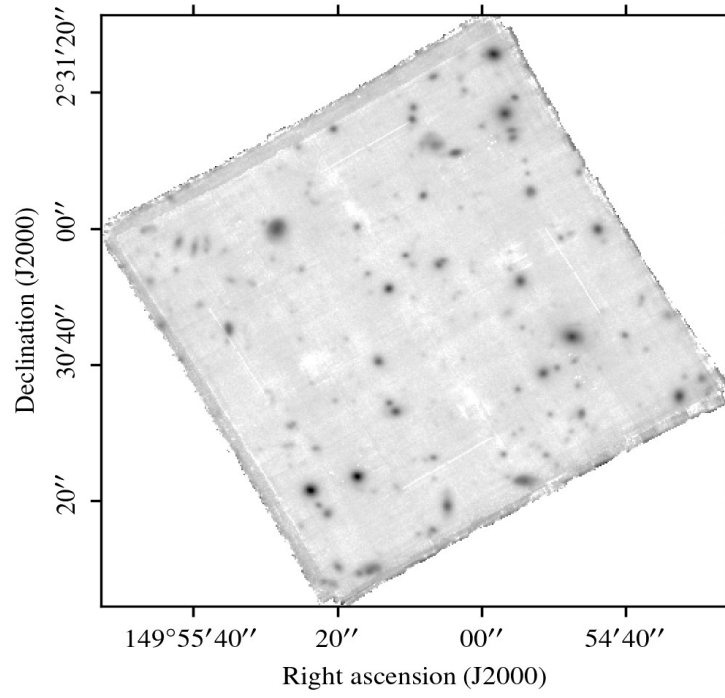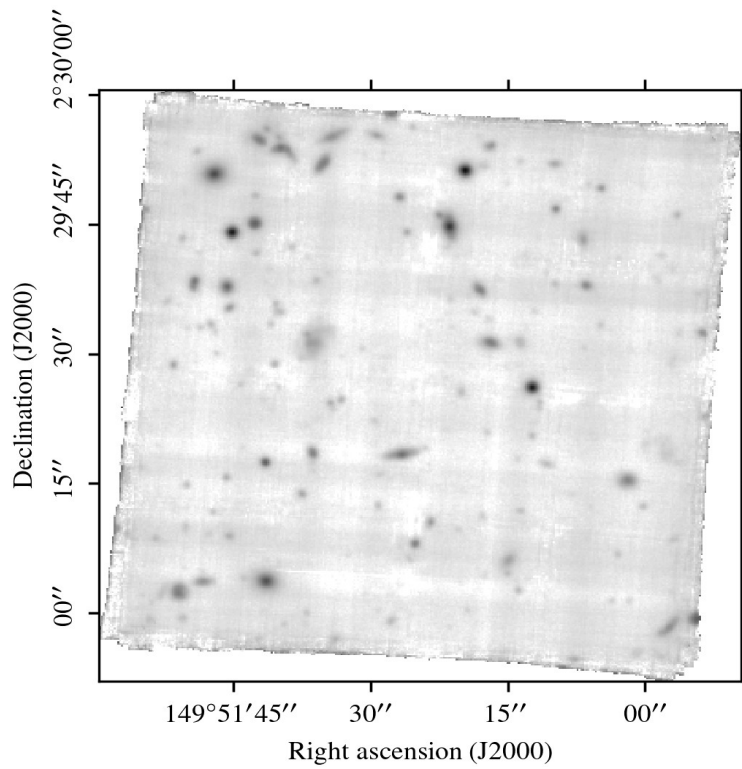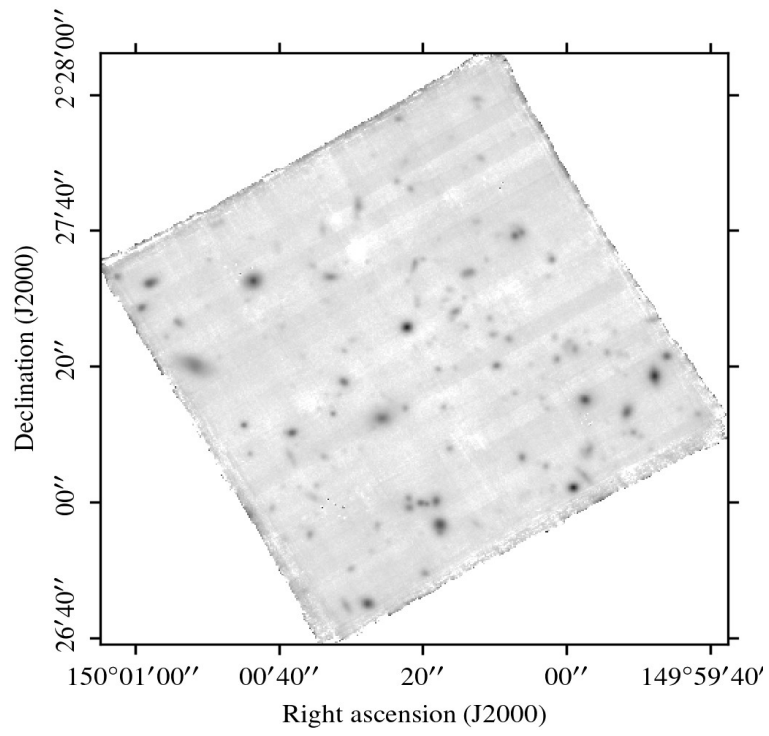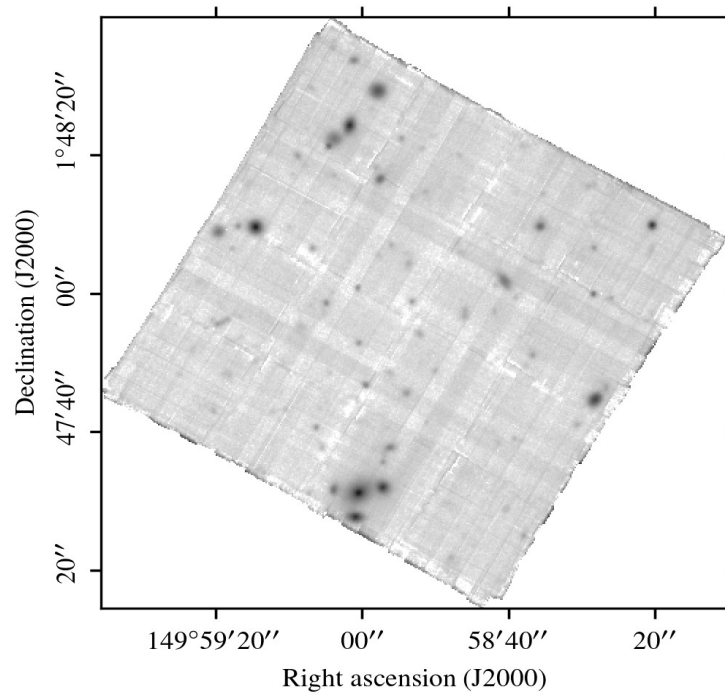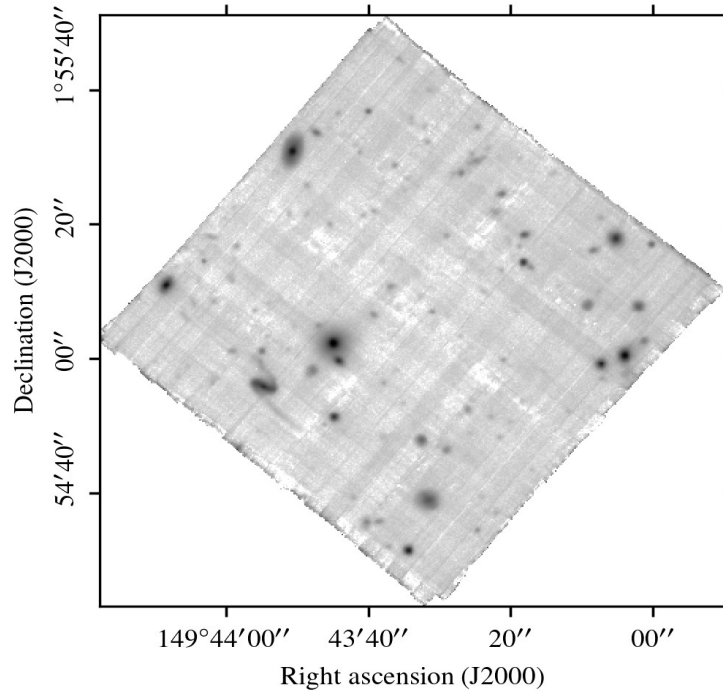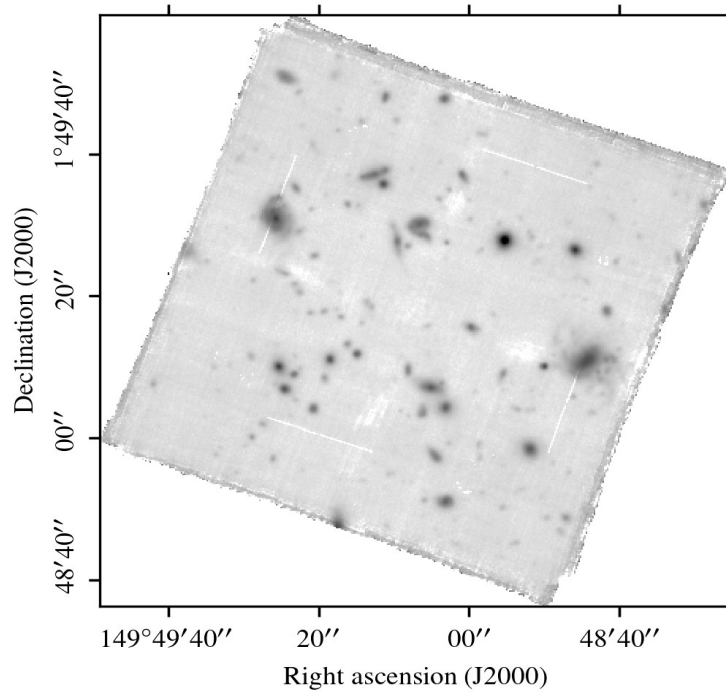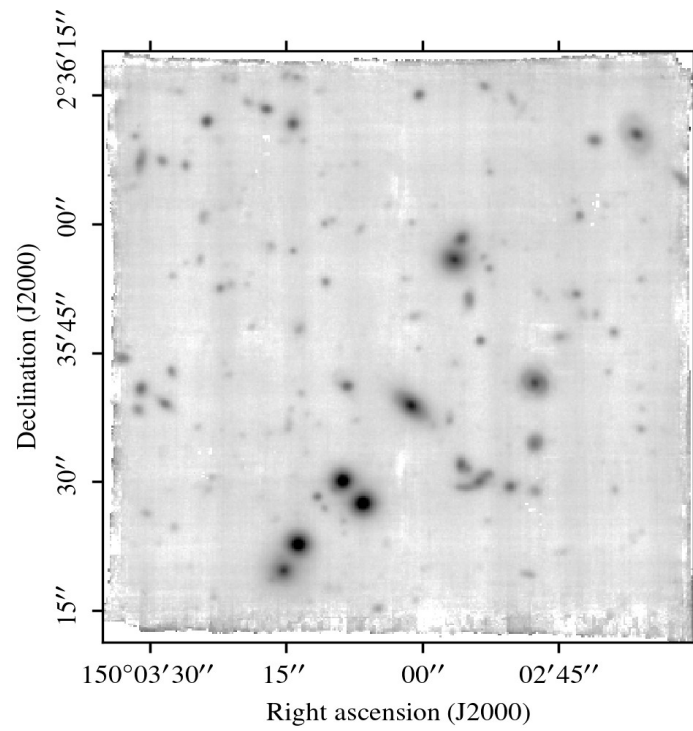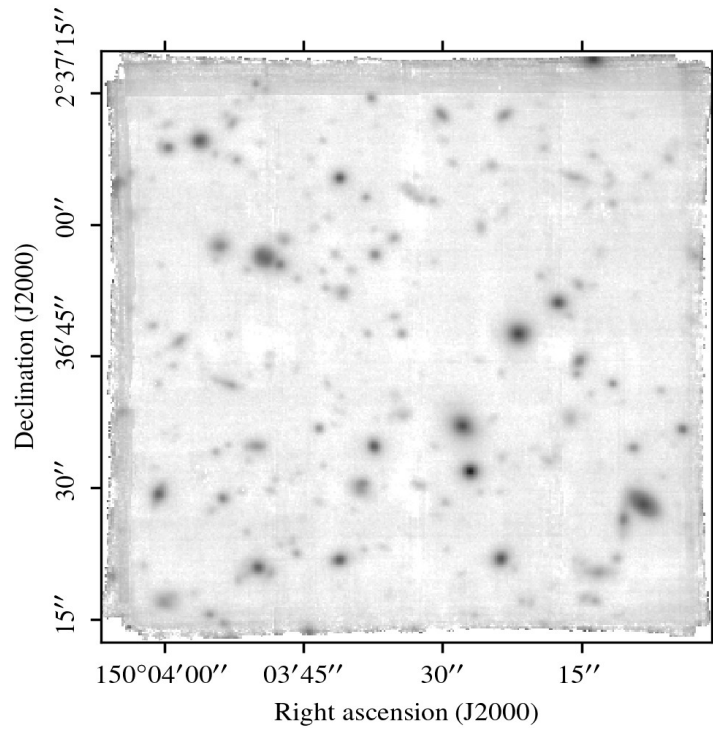

Fig. 8: White-light image in arbitrary logarithmic scale for [KLI2012] 32 field2 (CGr32-M2)

Fig. 9: White-light image in arbitrary logarithmic scale for [KLI2012] 32 field3 (CGr32-M3)

Fig. 10: White-light image in arbitrary logarithmic scale for [KLI2012] 34 (CGr34)

Fig. 11: White-light image in arbitrary logarithmic scale for [KLI2012] 35 (CGr35)

Fig. 12: White-light image in arbitrary logarithmic scale for [KLI2012] 51 (CGr51)

11

Fig. 13: White-light image in arbitrary logarithmic scale for [KLI2012] 61 (CGr61)

Fig. 14: White-light image in arbitrary logarithmic scale for [KLI2012] 79 (CGr79)

12

Fig. 15: White-light image in arbitrary logarithmic scale for [KLI2012] 84 field1 (CGr84-M1)

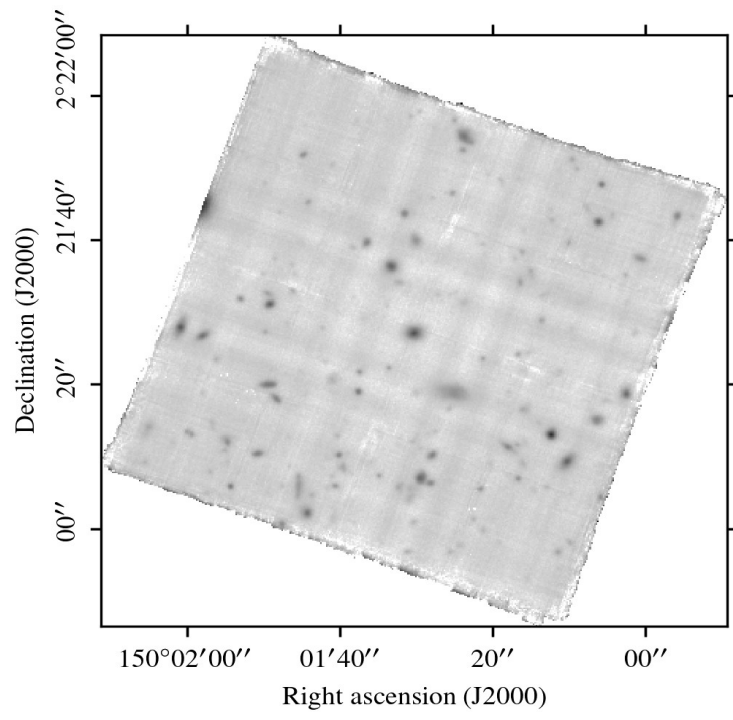*Fig. 16: White-light image in arbitrary logarithmic scale for [KLI2012] 84 field2 (CGr84-M2)*

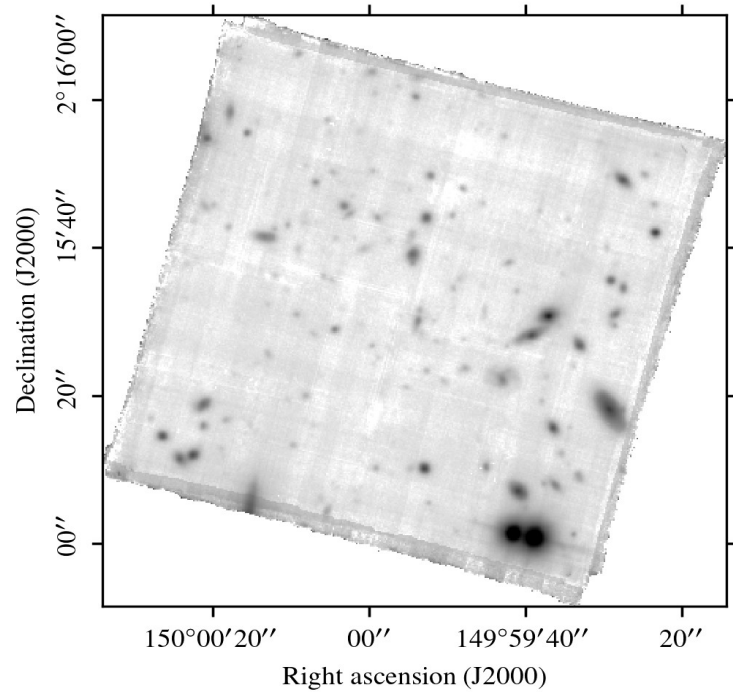*Fig. 17: White-light image in arbitrary logarithmic scale for [KLI2012] 87 (CGr87)*

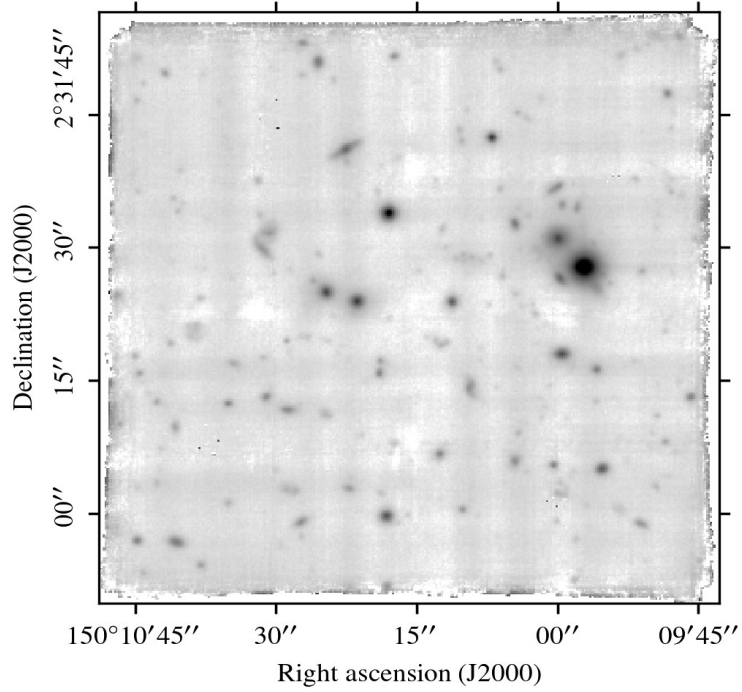*Fig. 18: White-light image in arbitrary logarithmic scale for [KLI2012] 114 (CGr114)*

14

Fig. 19: White-light image in arbitrary logarithmic scale for [KLI2012] 172 (CGr172)
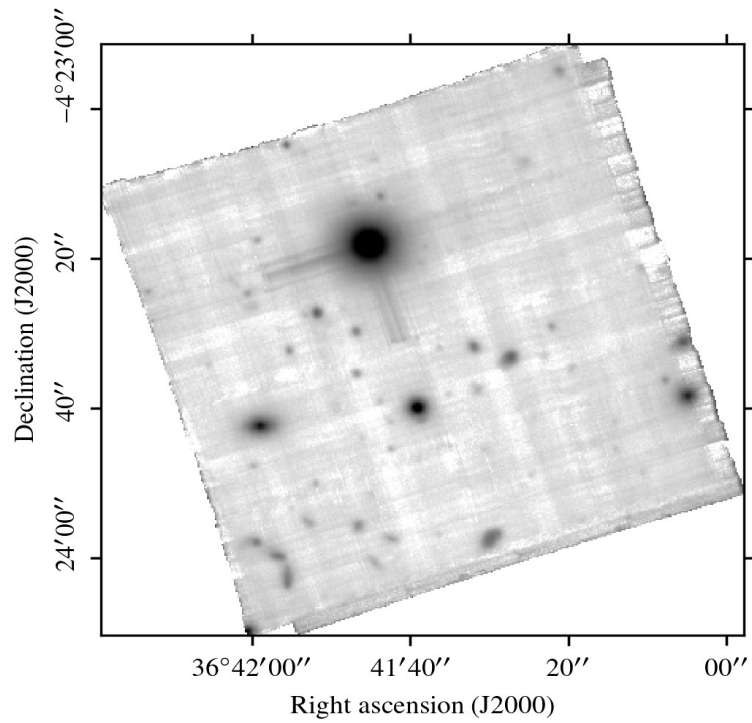

Fig. 20: White-light image in arbitrary logarithmic scale for [CMI2010] 189 (VGr189)